The Journal of Chemical Physics

RESEARCH ARTICLE | APRIL 22 2025

Selective formation and spectroscopic characterization of the $H_2CCS^{\bullet+}$ radical cation via dissociative ionization of thiophene

Jake A. Diprose ; Kim Steenbakkers ; Matteo Michielan ; Miroslav Polášek ; Daniela Ascenzi ; Sandra Brünken ; Claire Romanzin; Brianna R. Heazlewood ; Vincent Richardson

Check for updates

J. Chem. Phys. 162, 164304 (2025)
https://doi.org/10.1063/5.0260839

View Online
Export Citation

Articles You May Be Interested In

Velocity map imaging of OH radical products from IR activated $(CH_3)_2COO$ Criegee intermediates

J. Chem. Phys. (September 2016)

Combined crossed beam and theoretical studies of the $C(^1D) + CH_4$ reaction

J. Chem. Phys. (January 2013)

The vibrational bound states of isomerising disilyne

J. Chem. Phys. (August 2013)

25 April 2025 10:13:41

Webinar From Noise to Knowledge
May 13th – Register now
Zurich Instruments
Universität Konstanz

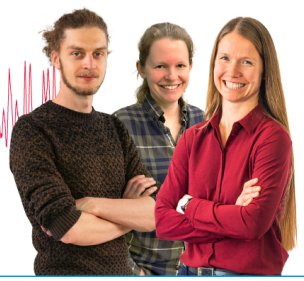

AIP Publishing

The Journal of Chemical Physics ARTICLE pubs.aip.org/aip/jcp

Selective formation and spectroscopic characterization of the $H_2CCS^{\bullet+}$ radical cation via dissociative ionization of thiophene

Cite as: J. Chem. Phys. 162, 164304 (2025); doi: 10.1063/5.0260839
Submitted: 27 January 2025 • Accepted: 31 March 2025 •
Published Online: 22 April 2025

View Online Export Citation CrossMark

Jake A. Diprose,[1] Kim Steenbakkers,[2] Matteo Michielan,[3] Miroslav Polášek,[4] Daniela Ascenzi,[3] Sandra Brünken,[2] Claire Romanzin,[5] Brianna R. Heazlewood,[1] and Vincent Richardson[1,a)]

AFFILIATIONS

[1] Department of Physics, University of Liverpool, Liverpool, United Kingdom
[2] Radboud University, FELIX Laboratory, Institute for Molecules and Materials, Toernooiveld 7, 6525 ED Nijmegen, The Netherlands
[3] Department of Physics, University of Trento, Trento, Italy
[4] J. Heyrovský Institute of Physical Chemistry of the Czech Academy of Sciences, Prague, Czechia
[5] Université Paris-Saclay, CNRS, Institut de Chimie Physique, Orsay, France/Synchrotron SOLEIL, L'Orme de Merisiers, Saint Aubin, France

[a)] **Author to whom correspondence should be addressed:** vincent.richardson@liverpool.ac.uk

ABSTRACT

The chemistry of sulfur-containing molecules is of significant interest to fields ranging from the combustion of petrochemicals to astrochemistry (with multiple S-containing species unambiguously detected in the interstellar medium or circumstellar shells). Here, infrared predissociation action spectroscopy and mass-analyzed ion kinetic energy spectroscopy measurements of the m/z 58 fragment from the dissociative ionization of thiophene are presented. Comparison is made between these experimental results and *ab initio* calculations (of both the spectral features and the fragmentation potential energy surface), which allows the fragment to be identified as the $H_2CCS^{\bullet+}$ radical cation. This conclusive identification addresses long-standing questions about the dissociative ionization of thiophene. The findings will enable further spectroscopic measurements and reactivity studies to be conducted, allowing $H_2CCS^{\bullet+}$ to be incorporated into models of astrochemical environments.

© 2025 Author(s). All article content, except where otherwise noted, is licensed under a Creative Commons Attribution (CC BY) license (https://creativecommons.org/licenses/by/4.0/). https://doi.org/10.1063/5.0260839

25 April 2025 10:13:41

I. INTRODUCTION

Thiophene (c–C_4H_4S), a five-membered heterocyclic aromatic compound, represents a fundamental unit found in a diverse range of chemical species and environments. Thiophene derivatives occur naturally in biologically active molecules such as plant metabolites[1] as well as being important precursors for the pharmaceutical and agrochemical industries[2–4] and ubiquitous building blocks in photonic materials such as organic photovoltaics and non-linear optical devices.[5] The physicochemical properties and UV photoabsorption and photoionization behavior are therefore a matter of great interest.[6]

Thiophenes and their derivatives are also the major aromatic sulfur heterocyclic contaminants found in fuels and petroleum products[7] and, as atmospheric and aqueous pollutants, can be released in urban and industrial areas by the incomplete combustion of fossil fuels, biomass burning, and marine oil spills. When emitted into the atmosphere, they are a major cause of acid rain and impact ozone, smog, and aerosol formation. While the removal of sulfur-containing molecules from fuels is necessary to improve combustion quality, conventional hydrodesulfurization methods are not effective at eliminating thiophenes from petroleum products due to the stability of the heteroaromatic ring. To facilitate effective purification methods, a more detailed understanding

© Author(s) 2025

of the chemical decomposition mechanisms of thiophene is required.[8,9]

Mass spectrometry-based techniques, usually coupled with separation methods such as gas chromatography or liquid chromatography, have become increasingly important in identifying heteroaromatic hydrocarbons and organosulfur components in complex mixtures.[10] Many of these techniques exploit the fragmentation behavior of molecular ions (e.g., by tandem mass spectrometry) to provide clues for the structures of the sulfur-containing compounds. A detailed understanding of decomposition mechanisms and the structures of the decomposing and fragment ions is therefore essential for the accurate interpretation of such data. In the case of thiophene, previous studies on the generation and fragmentation of the thiophene radical cation by collisions of thiophene with energetic particles, surfaces, and photons have been carried out both experimentally and theoretically.[6,11–19] However, no spectroscopic study has yet been performed to elucidate the structure of the ionic fragments.

Beyond their terrestrial implications, sulfur-containing molecules are relevant to the chemistry of the interstellar medium (ISM), where a plethora of S-containing species have been detected. Thiophene has not yet been observed in the ISM, as its detection via rotational spectroscopy is predicted to be challenging due to its small dipole moment (0.55 D),[20] but the presence of thiophene and methylthiophenes has been reported on the surface of Mars by the NASA Curiosity rover.[21,22] Alternatively, some protonated and substituted cyanothiophene derivatives possessing large dipole moments (e.g., 2- and 3-cyanothiophenes) might spontaneously form in the ISM and could be detected in the microwave range, as proposed by a recent quantum chemical investigation.[23]

In addition to S-containing heterocycles, there are several unsaturated linear S-containing species that have the potential to either form or be formed by S-containing heterocycles. Among them are polycarbon sulfides, a class of carbon chains that includes both neutral and charged species with the general formula H_xC_nS (x = 0–2 and n = 1–5). Non-hydrogenated neutral chains have been observed as large as n = 5,[24–29] with mono-hydrogenated neutrals observed up to n = 4,[26,30–32] and di-hydrogenated neutrals observed up to n = 3.[26,33] While ion observations are hindered by their typically low number densities and high reaction rates (resulting in shorter lifetimes) with respect to neutrals, mono-hydrogenated ions have been observed up to n = 3,[34,35] though no di-hydrogenated ions have yet been observed. Despite a lack of observation, the thioketene radical cation ($H_2CCS^{\bullet+}$) is a species of notable astrochemical interest following the recent observation of neutral thioketene (H_2CCS), the organosulfur equivalent of ketene (H_2CCO),[26] in a cold dark cloud.[36] In addition to the ionization of neutral thioketene [which has a vertical ionization energy (IE) of 8.89 eV][37–39] by Lyman-alpha photons, the protonation of recently detected HCCS[26] and the reactions of OCS^+ with C_2H_2 and of $C_2H_2^+$ with OCS[40–44] have been suggested as likely formation mechanisms under ISM conditions. Following the demonstration of synthetic pathways leading to thiophene and thioketene via the gas-phase reaction of S atoms with dienes such as 1,3-butadiene and isoprene,[45,46] the interconversion between these species also has significant implications for the build-up of organosulfur chemical complexity in the ISM.

In this work, we focus on the intense m/z 58 fragment ion formed by the dissociative ionization of thiophene.[15,16,19] The m/z 58 mass channel corresponds to the formation of one or more $[C_2H_2S]^{\bullet+}$ radical cation isomers via the elimination of C_2H_2. In addition to thioketene ($H_2C{=}C{=}S^{\bullet+}$), both thiirene (c-$CHCHS^{\bullet+}$) and ethynethiol ($HCCSH^{\bullet+}$) are known to be stable[44,47,48] and could contribute to this signal. Here, we seek to elucidate the fragmentation dynamics of thiophene for applications in analytical mass spectrometry and to demonstrate the selective generation of the $H_2CCS^{\bullet+}$ isomer for use in both high-resolution rotational spectroscopy and reactivity studies, contributing to ongoing astronomical observation and modeling efforts. To the best of our knowledge, information on the electronic states of the thioketene radical cation has only been inferred from the photoelectron spectrum of thioketene neutral H_2CCS.[37]

A multi-pronged approach is employed to examine both the fragmentation process itself and the structure of the resultant fragments. For the former, computational calculations on the fragmentation potential energy surface (PES) are combined with mass-analyzed ion kinetic energy (MIKE) spectroscopy, providing experimental verification of the calculated PES. For the latter, experimental infrared predissociation (IR-PD) spectra of the m/z 58 ions are recorded and compared with calculated line positions and intensities for the different isomers. While earlier studies have investigated HC_3S^+ ions using action spectroscopy,[49] the spectroscopic features of $H_2CCS^{\bullet+}$ have not previously been reported (to the best of our knowledge). Through the combination of spectroscopic measurements and detailed calculations set out in this work, the observed m/z 58 fragment is identified as $H_2CCS^{\bullet+}$.

II. EXPERIMENTAL AND COMPUTATIONAL METHODS

A. Experimental

1. Action spectroscopy

Experiments were performed using the FELion cryogenic ion trap apparatus at the Free Electron Lasers for Infrared eXperiments (FELIX)[50] Laboratory, which has been described in detail previously.[51] As such, only a brief description relating to the specific details of the current study is given here.

Thiophene, c–CHCHCHCHS, was introduced into the apparatus via evaporation of a pure liquid sample (Sigma-Aldrich, ≥99%). $[C_2H_2S]^{\bullet+}$ ions were produced from electron ionization (EI) of thiophene using both a standard EI source and a Storage Ion Source (SIS).[52] For the standard EI source, pressures used were on the order of 2×10^{-5} mbar, with electron energies in the ~30–40 eV range. For the SIS, a typical ion source pressure of 4×10^{-5} mbar was used, with electron energies also in the ~30–40 eV range. A mass spectrum of the ions generated using the EI source is shown in Fig. 1, with an equivalent spectrum for the SIS source given in Fig. S2 in the supplementary material. In both cases, an intense m/z 58 ion fragment is observed, indicative of an efficient fragmentation process.

Ions were extracted from the source in a 15 ms pulse and mass selected at m/z 58, corresponding to $[C_2H_2S]^{\bullet+}$ ions, using a quadrupole mass filter. Following mass selection, ions were guided into a cryogenic 22-pole ion trap,[53] which was maintained at a nominal temperature of ~12 K. Upon entering the trap, ions were cooled to the trap temperature through collisions with a 97:3 mixture of He:H_2, which was inserted into the trap via a pulsed piezo valve at a number density of ~10^{14} – 10^{15} molecules cm^{-3}. Each pulse was

25 April 2025 10:13:41

© Author(s) 2025

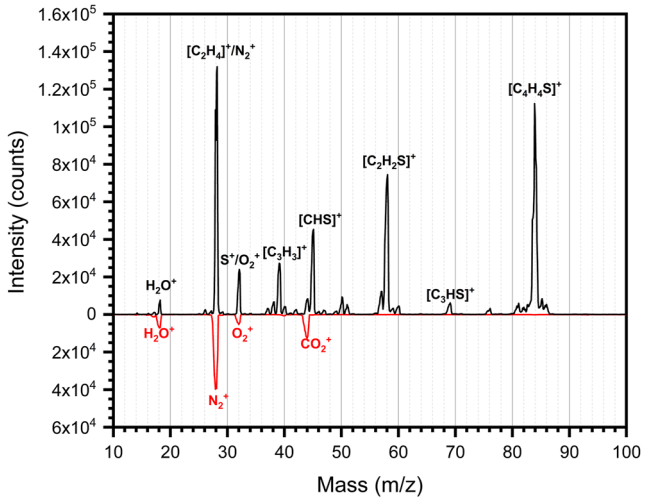

FIG. 1. Mass spectrum of the ions formed from thiophene using the ~30–40 eV EI source (black), compared to the background spectrum for this source (red, reflected below the axis) recorded prior to admission of thiophene.

triggered 15 ms before ions entered the trap and lasted for the duration of the ion pulse, allowing a high proportion (~15%) of the primary ions to form weakly bound complexes with H_2.

Comparison of the optimized mass spectrum recorded upon mass-selection of the *m*/*z* 58 ion fragments with that obtained following H_2-tagging is given in Fig. 2. The composition of the He:H_2 mixture was modified to optimize the proportion of singly-tagged ions, resulting in only a small proportion of multiply-tagged ions at successive 58 + 2*n* masses (where *n* is the number of attached H_2). Further details on the optimization of the tagging conditions are given in the supplementary material.

The small adjacent *m*/*z* 57 peak to the main *m*/*z* 58 peak can be explained by a combination of two different effects. First, the drift of the quadrupole resolution as a function of time can lead to the transmission of ions at adjacent masses to the target ion. Second, a small level of dissociation of the target ion may result from the collision of the ions entering the trap with the tagging pulse. As the *m*/*z* 58 signal is recorded as a depletion of the H_2-tagged *m*/*z* 60 channel, neither of these contributions to the adjacent *m*/*z* 57 channel are expected to influence the recorded spectra.

IR-PD spectra are measured as a depletion of the singly-H_2-tagged (*m*/*z* 60) ion mass signal as a function of laser frequency, with the absorption of resonant photons leading to the dissociation of the complex ions. The spectra presented here are given in terms of the measured depletion intensity on a per-photon basis, which allows for normalization of differences in laser power at different wavenumbers. Normalization of signal intensity *I* is performed following Eq. (1), where *S* is the observed ion counts, *B* is the baseline counts, *hν* is the photon energy, *E* is the laser pulse energy of a single shot (in mJ), and *N* is the number of shots:

$$I = -\frac{\ln(S/B)h\nu}{E \cdot N}. \quad (1)$$

IR radiation was provided by the FEL2 free-electron laser (FEL) present at the FELIX Laboratory operated at 10 Hz.[50] Different electron energy settings of the FEL were used to cover the appropriate wavelength range: for the low wavenumber (320–400 cm^{-1}) settings, macropulse energies of up to 3 mJ at the ion trap location were used; for the intermediate (400–1800 cm^{-1}) and high (2700–3500 cm^{-1}) wavenumber regions, energies of up to 8.4 and 4.1 mJ were utilized, respectively. Details of the laser full width at half maximum (FWHM) as a function of wavenumber are given in the supplementary material.

Saturation depletion measurements, an example of which is given in Fig. 3, were performed at different wavelengths (using both

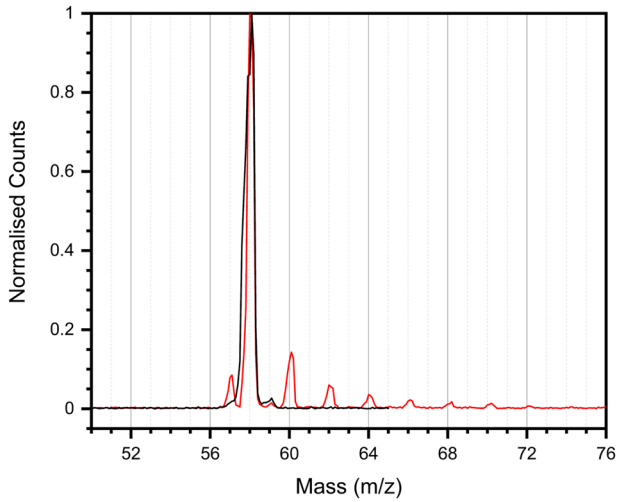

FIG. 2. Normalized mass spectra of mass-selected *m*/*z* 58 ions generated via the dissociative ionization of thiophene (c–CHCHCHCHS) using the EI source both before (black) and after H_2-tagging of these same ions (red).

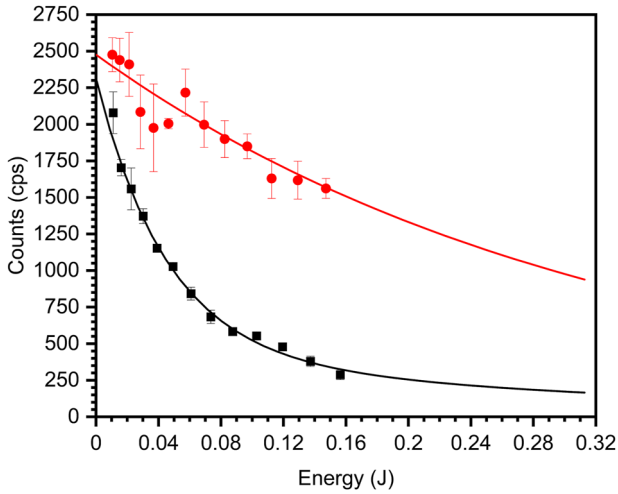

FIG. 3. Saturation depletion measurements of the tagged complexes as a function of the absorbed energy. Here, data are given off-resonance at 1624 cm^{-1} (red) and on-resonance at 1558 cm^{-1} (black).

25 April 2025 10:13:41

© Author(s) 2025

the EI and SIS sources) to quantify the isomeric composition, as has been described in detail elsewhere.[51,54] This involves irradiation of the tagged ions with a series of laser pulses resonant with an isomer-specific vibrational band, thereby leading to the complete dissociation of all H_2-tagged complexes of this isomer. The fractional abundance of the relevant isomer, A, is then determined by fitting the tagged mass ion signal as a function of the deposited energy using the following equation:

$$D = 1 - \frac{S}{B} = A \cdot (1 - e^{-k \cdot E \cdot N}), \quad (2)$$

where D is the depletion percentage and k is the efficiency of the IR-PD process for the band being probed. For all depletion values presented in this work, the given error is the sum of the fitting error and a systematic 5% uncertainty arising from an unknown combination of dark counts/noise from the detection systems and insufficient overlap between the irradiation and trapping regions that can prevent a small fraction of the trapped complexes being depleted while on-resonance.

2. MIKE spectroscopy

MIKE spectra have been recorded using a ZAB2-SEQ tandem mass spectrometer of reverse double-focusing geometry, in which the magnetic sector precedes the electrostatic sector. Precursor ions (c–CHCHCHCHS$^{\bullet+}$) were prepared by EI (70 eV, 150 °C) of neutral c–CHCHCHCHS (Merck, ≥99%). Following acceleration of 8 keV, precursor ions were mass-selected by the magnetic sector and allowed to dissociate spontaneously in the second field-free region of the instrument. The resultant ions were then analyzed by scanning the electrostatic sector. For peak profile measurements, the main beam width was reduced to 4 eV, corresponding to an energy resolution of 2000. For the m/z 58 ions ($[C_2H_2S]^{\bullet+}$), the metastable time window for ion fragmentation under these conditions was 9.7–18.8 μs.

B. Computational

Electronic structure calculations used to identify reaction intermediates and transition states relevant to the fragmentation of thiophene into $[C_2H_2S]^{\bullet+}$ isomers were performed with the Gaussian 16 suite of programs.[55] An initial mapping was performed at the B3LYP/cc-pVTZ level of theory, with the G4 level then used to obtain more accurate energies for the structures presented in this work. In all cases, open-shell species have been treated using unrestricted formalism (UB3LYP), with the closed-shell C_2H_2 molecule treated using restricted formalism (RB3LYP). The electronic structure calculations have been benchmarked by comparing the calculated IEs with those provided in the NIST WebBook[37,38,56] for a number of relevant structures, with the results shown in Table I.

Geometry optimization and subsequent harmonic and anharmonic vibrational frequency calculations for the open-shell $H_2CCS^{\bullet+}$ (C_{2v}, $^2B_1$), $HCCSH^{\bullet+}$ (C_S, $^2A''$), and c–$CHCHS^{\bullet+}$ (C_{2v}, $^2B_1$) isomers were again performed using the Gaussian 16 suite of programs.[55] All calculations were performed at the UB3LYP level of theory, using Dunning's cc-pVQZ[60,61] basis set, with a scaling factor of 0.969 applied[62] for comparison with the experimental spectra. The geometry of the $H_2CCS^{\bullet+}$–H_2 complex was calculated using the MOLPRO quantum chemistry software package, version 2015.1,[63,64] and optimized using the aug-cc-pVTZ[60,61,65] basis set, which includes diffuse functions to model long-range dispersive interactions. The obtained binding energy was counterpoise corrected to account for the basis set superposition error.

TABLE I. Comparison of IEs of thiophene (c–CHCHCHCHS), thioketene (CH_2CS), methylsulphide (CH_3SH), and dimethylsulphide (CH_3SCH_3) calculated at the B3LYP/cc-pVTZ and G4 levels of theory (at 0 K) with the reference IEs from the NIST WebBook.[37,38,56]

Species	Ionization energy (eV)		
	NIST	B3LYP/cc-pVTZ	G4
Thiophene	8.86 ± 0.02[a]	8.67	8.95
Thioketene	8.77[b]	8.84	8.89
Methylsulphide	9.439 ± 0.005[c]	9.32	9.44
Dimethylsulphide	8.69 ± 0.02[d]	8.53	8.68

[a]A recent determination (not reported in NIST) gives an adiabatic IE of 8.8742 ± 0.0002 eV.[57]
[b]In NIST, Refs. 37 and 38 are provided as a source for this IE, though no adiabatic value is reported in either paper. The value is expected to have been assigned using the onset of the PE band in the spectrum shown in Ref. 37.
[c]A recent determination (not reported in NIST) gives an IE of 9.454 58 ± 0.000 36 eV.[58]
[d]A recent determination (not reported in NIST) gives an adiabatic IE of 8.6903 ± 0.0009 eV.[59]

III. RESULTS

A. Fragmentation potential energy surface (PES)

The fragmentation of the thiophene ion (c–CHCHCHCHS$^{\bullet+}$), hereafter referred to as **A1**, into $[C_2H_2S]^{\bullet+}$ and C_2H_2 has been explored at both the B3LYP and G4 levels of theory, with the results of the higher-level (G4) calculations provided in this section (comparison of the two levels of theory is given in the Computational Methods section). Energies for each structure are given, in parentheses, in kJ mol^{-1} relative to the energy of **A1**. The PES is shown graphically in Fig. 4, with the structures of all relevant identified intermediates and transition states provided in the supplementary material (in Figs. S11–S31, with geometries in Å given in Tables S8–S28).

The lowest energy pathway leading to the formation of the most stable isomer, the thioketene radical cation $[H_2CCS]^{\bullet+}$, proceeds from **A1** via an initial [1,2] H-shift to give c–$CCH_2CHCHS^{\bullet+}$ (186), hereafter referred to as **A2**, via **A1-2** (239). **A2** can then ring open through cleavage of the S–CH bond via **A2-3** (275) to give $CHCHCH_2CS^{\bullet+}$ (243), hereafter referred to as **A3**. Further cleavage of the CH_2–CH bond via **A3-4** (300) yields **A4** (284), a van der Waals cluster of $H_2CCS^{\bullet+}$ and C_2H_2 that can fragment into the separated products (307) without a barrier. This pathway is shown with pink lines in Fig. 4.

The next lowest energy pathway (blue lines in Fig. 4) involves the direct ring opening of **A1** through the cleavage of one of the S–CH bonds via **A1-5** (356) to give $CHCHCHCHS^{\bullet+}$ (334), hereafter referred to as **A5**. Further cleavage of the central CH–CH bond via **A5-6** (392) gives **A6** (336), a van der Waals cluster of c–$CHCHS^{\bullet+}$ and C_2H_2 that can fragment into the separated products (366) without a barrier.

25 April 2025 10:13:41

© Author(s) 2025

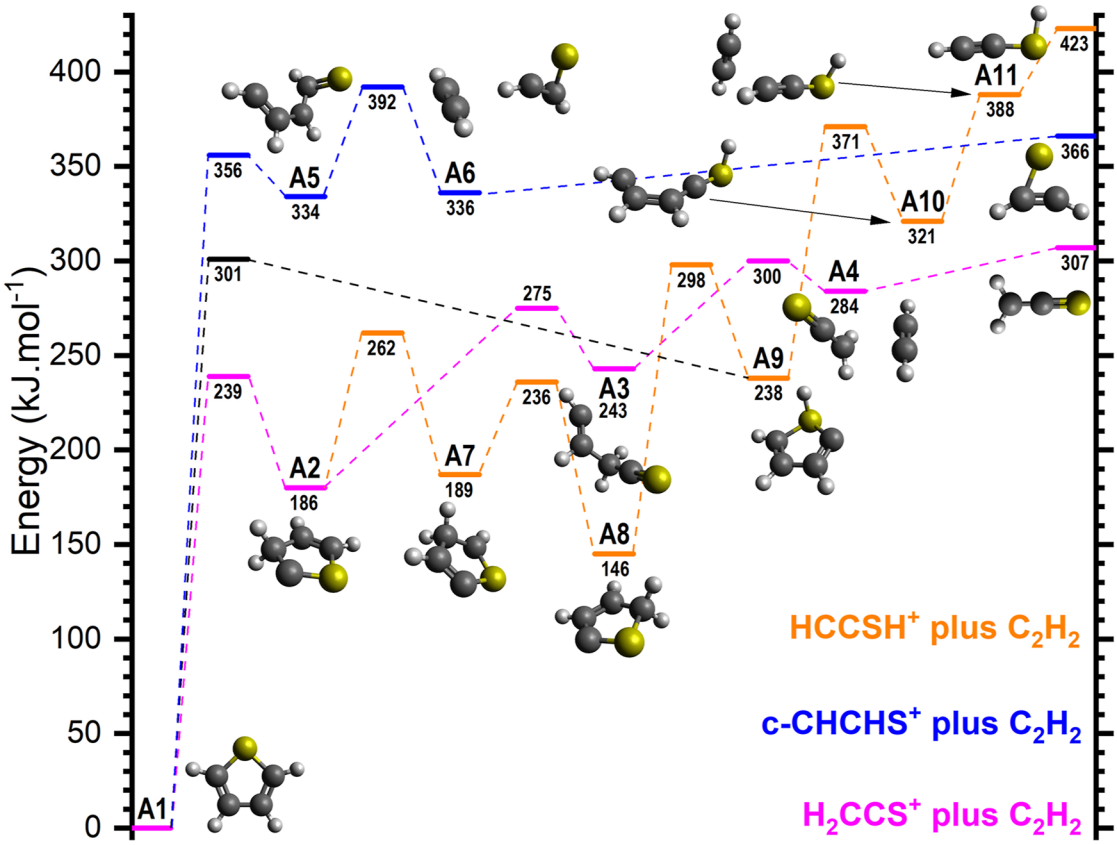

FIG. 4. Intermediate structures and transition states, calculated at the G4 level of theory, relevant to the fragmentation of the thiophene radical cation (c–CHCHCHCHS$^{\bullet+}$, **A1**) into the $H_2CCS^{\bullet+}$, c–CHCHS$^{\bullet+}$, and HCCSH$^{\bullet+}$ isomers of $[C_2H_2S]^{\bullet+}$.

The final isomer of $[C_2H_2S]^{\bullet+}$ for which a pathway has been identified is HCCSH$^{\bullet+}$, which is shown with orange lines in Fig. 4. The lowest energy pathway involves a series of [1,2] H-shifts from **A2**, beginning with a shift to give c–CCHCH$_2$CHS$^{\bullet+}$ (189), hereafter referred to as **A7**, via **A2-7** (262). **A7** can then undergo a further shift via **A7-8** (236) to give c–CCHCHCH$_2$S$^{\bullet+}$ (146), hereafter referred to as **A8**. **A8** can then undergo a final [1,2] shift to give c– CCHCHCHSH$^{\bullet+}$ (238), hereafter referred to as **A9**, via **A8-9** (298).

A9 can also be reached directly from **A1** through a [1,2] H-shift via **A1-9** (301). Though this second pathway is slightly higher in energy (by 3 kJ mol^{-1}), the far fewer interconversions required may mean this is a more feasible pathway for the formation of **A9** from **A1**. However, a detailed investigation of the relative contributions of these two pathways to the potential formation of HCCSH$^{\bullet+}$ from thiophene is beyond the scope of this work. From **A9**, cleavage of the S–CH bond via **A9-10** (371) gives CHCHCHCSH$^{\bullet+}$ (321), hereafter referred to as **A10**. No transition state has been found for the cleavage of the central CH–CH bond, but a subsequent van der Waals complex of HCCSH$^{\bullet+}$ and C_2H_2 (388), hereafter referred to as **A11**, has been identified. This can then dissociate into the separated products (423) without a barrier.

The fragmentation PES of the thiophene cation has been studied previously at both the B3LYP/6-311+G(3df,3pd)[14,15] and G4 levels of theory.[11] In the former studies,[14,15] only the fragmentation pathway yielding $H_2CCS^{\bullet+}$ was considered, while Ref. 11 also identified a pathway leading to HCCSH$^{\bullet+}$, but neither previous study identified a pathway leading to the formation of c–CHCHS$^{\bullet+}$. An earlier study[14] also identified **A2** as the initial intermediate, with previously calculated energies of 248 and 187 kJ mol^{-1} (for **A1-2** and **A2**, respectively), in good agreement with the values presented here. From **A2**, calculations[14] predicted a second ring-opened intermediate ($H_2CCSCHCH^{\bullet+}$) formed by rupture of a C–C bond, which requires overcoming a TS at high energy (343 kJ mol^{-1}) before leading to products. However, this calculated prediction was inconsistent with experimental molecular ion breakdown curves. Hence, they concluded that the most plausible mechanism is not stepwise C–C bond cleavage followed by C_2H_2 elimination but a concerted breaking of both a C–C and C–S bond, leading directly to products from the **A2** intermediate, even though the details of such a concerted process were not specifically identified.[14]

A more recent theoretical study,[11] performed at the same level of theory as this work, also identified a fragmentation channel

25 April 2025 10:13:41

© Author(s) 2025

proceeding to $H_2CCS^{\bullet+}$ plus C_2H_2 via **A2** and **A3**, but found no barrier to interconversion between **A2** and **A3**, or from **A3** to product formation. Similarly, while this previous study identified a pathway to form $HCCSH^{\bullet+}$ via **A9** and **A10**, this was again found to be without barriers to interconversion following the formation of **A9**. While the calculated energies of the common structures show a good level of agreement (within 6–8 kJ mol^{-1}) with the work presented here, several reaction pathways identified in this work (e.g., the formation of $c–CHCHS^{\bullet+}$ and the lower-energy pathway to form $HCCSH^{\bullet+}$ via **A7** and **A8**) were not reported.

B. MIKE spectroscopy

To probe the metastable decomposition pathways detailed in Fig. 4, MIKE spectra have been recorded for $c–CHCHCHCHS^{\bullet+}$ ions generated via dissociative ionization of neutral thiophene (c–CHCHCHCHS), with the results shown in Fig. 5. The full kinetic energy release (KER) distribution of the *m*/*z* 58 fragment ion has been determined from the metastable peak shapes using the META algorithm described in Szilágyi and Vékey.[66] The *m*/*z* 58 peak, corresponding to the loss of C_2H_2, has a sharp profile, characteristic of a process that involves a small KER and exhibits a narrow KER distribution, consistent with previous MIKE spectroscopy measurements.[19] The obtained KER distribution of the *m*/*z* 58 fragment ion is given in Fig. 6. A discussion of these results in light of the calculated PES is given in Sec. IV.

C. Spectroscopy of $[C_2H_2S]^{\bullet+}$

The experimental IR-PD spectrum of the *m*/*z* 58 fragment in the explored wavelength ranges (320–1800 and 2700–3500 cm^{-1}) is shown in Fig. 7, where it is compared to the computed spectral features for the $H_2CCS^{\bullet+}$, $c–CHCHS^{\bullet+}$, and $HCCSH^{\bullet+}$ isomers. Line positions and intensities have been calculated at the UB3LYP/cc-pVQZ level of theory. Assignment and isomeric verification are discussed below and made on the basis of direct

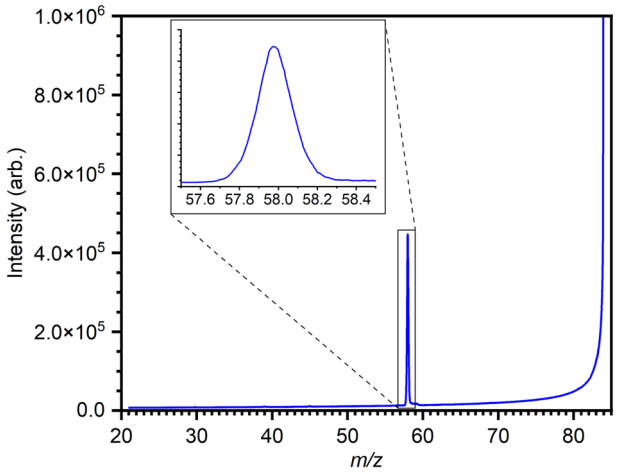

FIG. 5. Mass-analyzed ion kinetic energy (MIKE) spectrum of the *m*/*z* 58 ion formed via dissociative ionization of thiophene. The inset shows an enlarged view of the shape of the *m*/*z* 58 peak.

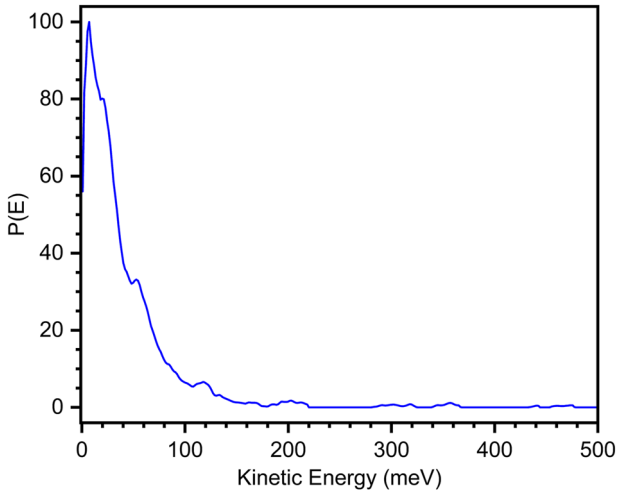

FIG. 6. Kinetic energy release distribution of *m*/*z* 58 ion fragments ($[C_2H_2S]^{\bullet+}$) from the dissociative ionization of thiophene ($c–CHCHCHCHS^{\bullet+}$).

comparison of the experimental band positions with the calculated frequencies and intensities. The experimental spectral features (line positions, FHWM, and relative intensities), obtained by fitting the observed features with Gaussian functions, are summarized in Table II along with the calculated line positions and intensities for the $H_2CCS^{\bullet+}$ isomer. The relative intensities have been normalized to the calculated numerical values with respect to the C–C–S stretching mode (ν_2). Calculated line positions and intensities for the $c–CHCHS^{\bullet+}$ and $HCCSH^{\bullet+}$ isomers are given in Tables S2 and S3 of the supplementary material. Overall, we note a high level of agreement between the experimental spectrum and the calculated $H_2CCS^{\bullet+}$ transitions; there are no clear experimental features corresponding to the $HCCSH^{\bullet+}$ or $c–CHCHS^{\bullet+}$ isomers, indicative of largely selective formation processes.

The only features observed in the low (<400 cm^{-1}) wavenumber region comprise the double-peaked band at 331(3) and 340(2) cm^{-1}, in good agreement with the computed line positions for the in- and out-of-plane C–C–S bending modes of $H_2CCS^{\bullet+}$ at 336.6 and 341.3 cm^{-1} (ν_9 and ν_6), respectively. While the two contributions to the experimental feature are not easily apparent on first inspection, reasonable fitting was only possible with a double Gaussian. The presence of a double feature is further evidenced by the observed feature being markedly broader than the FELIX intrinsic line width in this region (~4 cm^{-1}). Importantly, no features in this region are predicted for the $c–CHCHS^{\bullet+}$ isomer (the lowest wavenumber feature is at 633 cm^{-1}), while the predicted features for the $HCCSH^{\bullet+}$ isomer are at 273 and 310 cm^{-1}. However, we note that the presence of one or both of $c–CHCHS^{\bullet+}$ and $HCCSH^{\bullet+}$ cannot be dismissed on this basis, as there are no predicted strong features for either isomer in this wavenumber region.

In the intermediate (~400–1800 cm^{-1}) region, we observe four distinct features. The most intense is assigned to the C–C–S stretch of $H_2CCS^{\bullet+}$ and is observed at 1555(2) cm^{-1}, which is in good agreement with the calculated line position of 1548.4 cm^{-1} (ν_2). A further clear feature, assigned to the H–C–H in-plane scissoring mode, is

25 April 2025 10:13:41

© Author(s) 2025

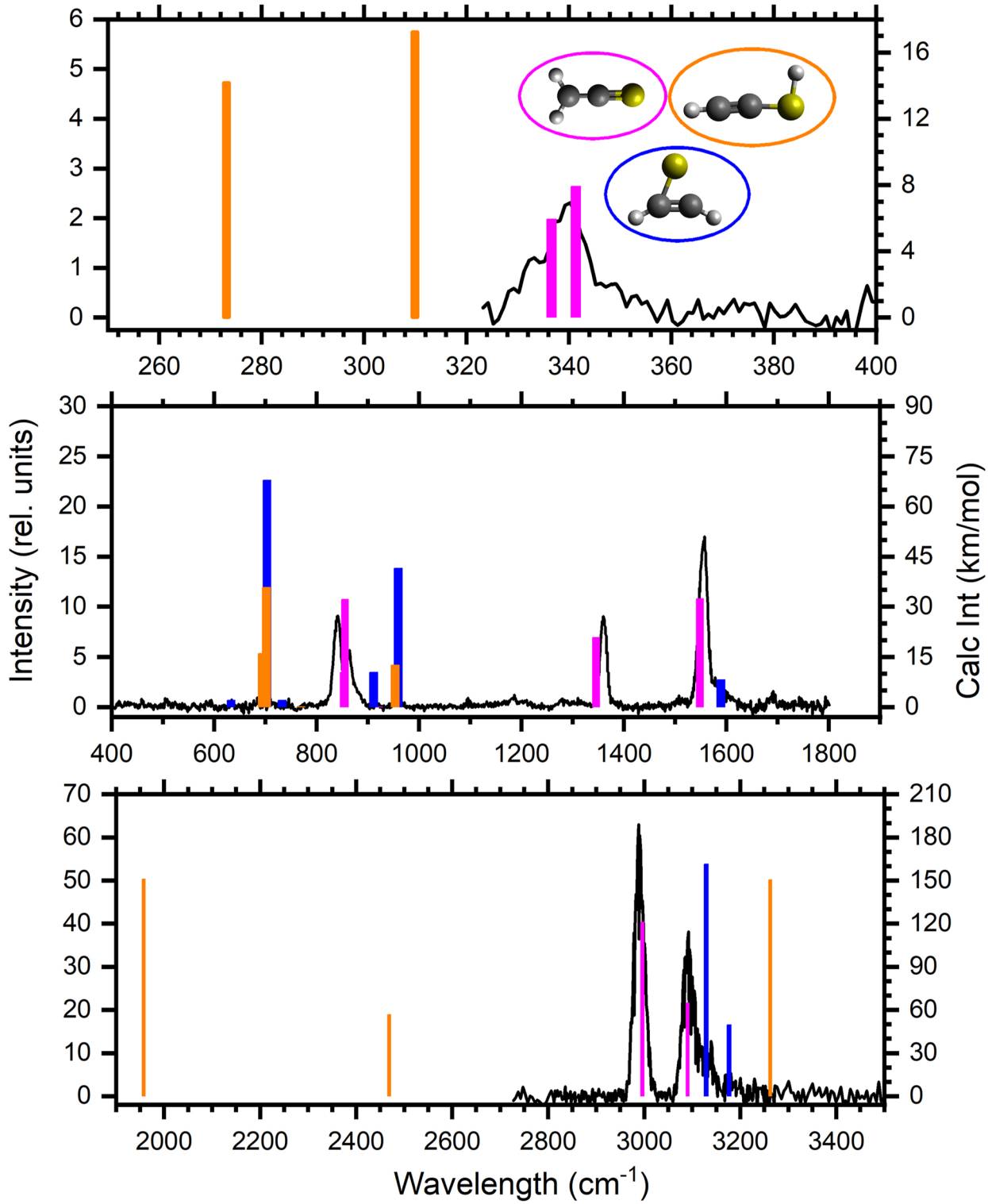

FIG. 7. IR-PD vibrational spectra of the *m*/*z* 58 fragment from dissociative ionization of thiophene: experimental results are given in black, while the computed line positions and intensities (calculated at the UB3LYP/cc-pVQZ level of theory) of the linear $H_2CCS^{\bullet+}$, linear $HCCSH^{\bullet+}$, and cyclic c–$HCHCS^{\bullet+}$ isomers are shown in pink, orange, and blue, respectively.

25 April 2025 10:13:41

© Author(s) 2025

TABLE II. Experimental IR band positions (in cm^{-1}) and intensities (in relative units) are compared with calculated harmonic values for the linear $H_2CCS^{\bullet+}$ isomer (where intensities are given in km mol^{-1}). Predicted fundamental frequencies are given for the bare cation structure at the UB3LYP/cc-pVQZ level of theory, with vibrational scaling factors applied, and symmetries provided.[62] Uncertainties are provided in parentheses for the last digit, with all experimental line positions determined by fitting each peak with a Gaussian function. The relative intensities have been normalized to the calculated numerical values with respect to the C–C–S stretching mode (ν_2).

Mode	Symmetry	IR-PD frequency (cm^{-1})	IR-PD intensity rel.	Depletion (%)	Calc. frequency (cm^{-1})	Calc. intensity (km/mol)
C–C–S bend in-plane (ν_9)	B_2	331(3)	0.3(1)	···	336.6	5.9
C–C–S bend out-plane (ν_6)	B_1	340(2)	1.9(2)	···	341.3	7.9
H–C–H wagging out-of-plane (ν_5)	B_1	840(2)	13.6(3)	···	855.5	32.2
C–S stretch (ν_4)	A_1	864(2)	8.4(3)	85(6)	853.3	10.4
H–C–H rocking in-plane (ν_8)	B_2	···	···	···	922.2	0.0
H–C–H in-plane scissoring (ν_3)	A_1	1360(2)	12.8(2)	···	1346.1	20.9
C–C–S stretch (ν_2)	A_1	1555(2)	32.1(2)	80(7)	1548.4	32.4
H–C–H stretch (ν_1)	A_1	2990(3)	127(3)	85(6)	2996.0	121.1
H–C–H stretch (ν_7)	B_2	3090(4)	94(4)	···	3090.2	64.8

observed at 1360(2) cm^{-1}, in reasonable agreement with the calculated line position of 1346.1 cm^{-1} (ν_3). The final two features in this region are less clearly interpreted. Scaled harmonic calculations predict a line at 853.3 cm^{-1} corresponding to the C–S stretching mode (ν_4), with a more intense line at 855.5 cm^{-1} corresponding to the out-of-plane H–C–H wagging mode (ν_5). Experimentally, however, while we do observe a pair of bands in this region, we observe the more intense of these at 840(2) cm^{-1}, with the less intense feature at 864(2) cm^{-1}.

To better understand these features, we performed additional anharmonic calculations (again at the UB3LYP/cc-pVQZ level of theory) for the three isomers, with full details provided in Tables S4–S6 of the supplementary material. While deviations between the harmonic and anharmonic calculations are limited, for the anharmonic calculations, the relative positions of these two features are inverted, as shown in Fig. 8. Although the calculated anharmonic line positions are slightly shifted with respect to experiment (the C–S stretching mode is predicted at 879.2 cm^{-1} and the H–C–H wagging mode at 864.6 cm^{-1}), the separation of ~15 cm^{-1} is in excellent agreement with the experimental separation of 14 cm^{-1}. Given this and the comparatively small predicted separation of the two bands of 0.3 cm^{-1}, we assign the more intense feature at 840(2) cm^{-1} to the H–C–H wagging mode, while the 864(2) cm^{-1} feature is assigned to the C–S stretching mode.

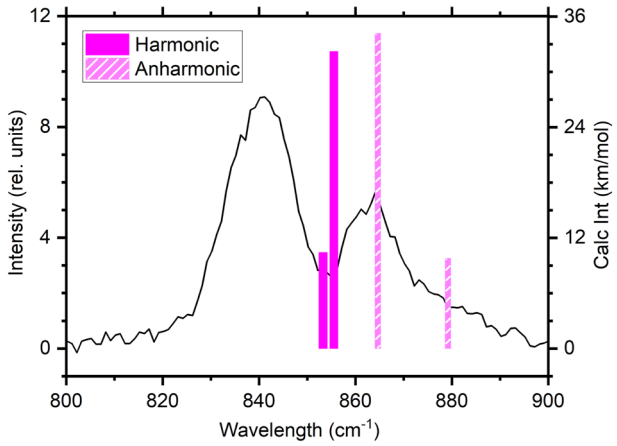

FIG. 8. IR-PD vibrational spectra in the 800–900 cm^{-1} range of the *m*/*z* 58 fragment from dissociative ionization of thiophene: experimental results are given in black, alongside the calculated harmonic (solid dark pink) and anharmonic (dashed light pink) positions and intensities for the $H_2CCS^{\bullet+}$ isomer.

Finally, in the higher wavenumber (~2800–3300 cm^{-1}) region, we observe an intense feature at 2990(3) cm^{-1} assigned to the H–C–H symmetric stretch, in excellent agreement with the calculated line position of 2996.0 cm^{-1} (ν_1). A less intense band, observed at 3090(4) cm^{-1}, is also in excellent agreement with the calculated line position of 3090.2 cm^{-1} for the H–C–H antisymmetric stretch (ν_7).

Given the excellent agreement between the calculated frequencies of the bare ion and the experimental IR-PD spectrum, it is anticipated that the H_2 tag has minimal influence on the vibrational structure. To confirm this, a geometry search was conducted to determine the H_2 binding position and calculate its binding energy, with the results given in Fig. S10 of the supplementary material. The minimum energy configuration was found with H_2 attached along the molecular symmetry axis to the hydrogen atoms of $H_2CCS^{\bullet+}$, with the H–H bond out of the plane. At this position, the binding energy was only 200 cm^{-1}, consistent with the expected negligible effect of the tag on the positions of the vibrational transitions.

The experimental spectrum therefore points toward the exclusive formation of $H_2CCS^{\bullet+}$ as the dominant ion in the dissociative ionization of thiophene, as no features of the higher-energy isomers could be detected. As an additional test to determine the isomeric composition, depletion measurements have been performed at 845, 1558, and 2990 cm^{-1}, with respective isomeric purities of 0.85(6), 0.80(7), and 0.85(6). Further consideration of these values is given in Sec. IV. Furthermore, to confirm that the EI and SIS sources can be used interchangeably, depletion measurements of the intense ~1560 cm^{-1} line have been performed using both sources, with isomeric purities of 0.83(6) and 0.79(6) obtained using the EI and SIS sources,

25 April 2025 10:13:41

© Author(s) 2025

respectively. From this, we conclude that the isomeric purity is independent of the source used, and no further distinction between the two datasets is made. A direct comparison of the spectra obtained using the two sources in the 700–1800 cm^{-1} region is given in Fig. S3 of the supplementary material, with the depletion plots for the 845, 1558 (using both EI and SIS sources), and 2990 cm^{-1} bands shown in Fig. S4 of the supplementary material.

IV. DISCUSSION

The objective of this study is to perform a conclusive isomeric identification of the m/z 58 fragment of thiophene and to provide new insights into the underlying fragmentation mechanism(s). To do so, we have compared experimental and calculated infrared spectra and considered the energetics of the fragmentation process through PES calculations and MIKE spectroscopy. The combination of these approaches provides a rigorous description of both the fragmentation process and the identity of the fragmentation products.

The measured IR-PD spectra display a high level of agreement with the calculated $H_2CCS^{\bullet+}$ spectral features. All notable features of the experimental spectra are matched by predicted line positions, with the only predicted feature that is not clearly observed being the in-plane H–C–H rocking mode. As this mode has a predicted intensity of 0.0 km mol^{-1}, the lack of a clear feature corresponding to the predicted line position of 922.2 cm^{-1} is unsurprising. While small shifts are observed throughout (the largest being 16 cm^{-1} with an average shift of 8 cm^{-1}), these are fully consistent with the experimental spectrum within the expected level of accuracy of the calculations. Although there is a greater variation between the calculated and experimental relative intensities, the order of peak intensities is the same for both experimental and calculated harmonic spectra, with the sole exception of the C–S stretching (ν_2) and H–C–H out-of-plane wagging (ν_5) modes. However, a match with the experimental relative positions is well reproduced by anharmonic calculations of these two features, with the shift in the C–S stretching (ν_2) frequency indicative of a notable anharmonic component to this mode.

From the depletion measurements shown in the supplementary material, the results of which are summarized in Table II, we conclude that the $H_2CCS^{\bullet+}$ isomer constitutes at least 80(7)% of the m/z 58 fragment signal. However, the lack of complete depletion for the main spectroscopic features of the $H_2CCS^{\bullet+}$ isomer necessitates consideration of other potential contributors to this mass channel. From the comparison between the experimental spectrum and those calculated for the c–CHCHS$^{\bullet+}$ and HCCSH$^{\bullet+}$ isomers shown in Fig. 7, we conclude that there is little spectroscopic evidence of either of the two isomers. While we note a good agreement between the shoulders of the 1555 and 3090 cm^{-1} peaks and the predicted c–CHCHS$^{\bullet+}$ features at 1589.5 and 3128.8 cm^{-1}, respectively, no experimental matches are found for the intense 703.2 and 959.6 cm^{-1} features predicted for this isomer. We, therefore, conclude that the remaining ion signal at this mass is the result of an unknown combination of minor contributions from one or both of the higher-energy isomers, isobaric contamination, dark counts, and potential insufficient overlap between the irradiation and trapping regions that can prevent a small fraction of the trapped complexes being depleted even while on-resonance.

The spectroscopic characterization is supported by the calculated PES shown in Fig. 4. The formation of the $H_2CCS^{\bullet+}$ isomer is significantly lower in energy than the formation of the c–CHCHS$^{\bullet+}$ and HCCSH$^{\bullet+}$ isomers, by 59 and 116 kJ mol^{-1} respectively, though all three pathways are formally accessible at the electron energies used to ionize thiophene. Furthermore, while the formation of both the $H_2CCS^{\bullet+}$ and HCCSH$^{\bullet+}$ isomers proceeds without a barrier with respect to the product fragments, the formation of the c–CHCHS$^{\bullet+}$ isomer involves a reverse activation barrier of 26 kJ mol^{-1}. Given this, and the fact that the $H_2CCS^{\bullet+}$ formation pathway does not involve significantly more interconversions (4) than for the other two isomers (3 and 4/7, respectively), the fragmentation is expected to significantly favor the $H_2CCS^{\bullet+}$ isomer.

This argument is supported by the MIKE spectra, where the width of the observed KER distribution depends on the energy of the products relative to the maximum barrier heights. The observed narrow KER distribution for the m/z 58 fragment of thiophene is consistent with a continuously endothermic fragmentation process without a discernible reverse activation barrier, in agreement with previous photoion-photoelectron coincidence (PIPECO) and MIKE spectroscopy studies.[19] The absence of a reverse activation barrier aligns with the calculated pathways for the $H_2CCS^{\bullet+}$ and HCCSH$^{\bullet+}$ isomers but not with the pathway leading to c–CHCHS$^{\bullet+}$ formation, where the energy of the transition state **A5-6** is 26 kJ/mol^{-1} higher than the energy of c–CHCHS$^{\bullet+}$ plus C_2H_2 products.

The identification of $H_2CCS^{\bullet+}$ as the major contributor to the m/z 58 fragment signal is consistent with both the calculated PES and previous experimental observations.[14–16,19] The continuously endothermic pathway leading to HCCSH$^{\bullet+}$ that has been identified both here and in a recent computational study[11] is also inconsistent with a reverse activation barrier and, by extension, consistent with the MIKE spectra reported here and previously.[19] However, despite previous assumptions to the contrary,[15] no evidence of this isomer is observed spectroscopically. To the best of our knowledge, no pathway leading to the formation of the c–CHCHS$^{\bullet+}$ isomer has been identified previously, with these details reported for the first time here. However, the higher energy nature of this pathway and the presence of a reverse activation barrier prevent it from being energetically accessible at the onset of the m/z 58 signal.

V. CONCLUSIONS

We present the first spectroscopic identification of the thioketene radical cation ($H_2CCS^{\bullet+}$) as the major contributor to the intense m/z 58 fragment signal from the thiophene cation. The conclusive identification of the m/z 58 fragment as $H_2CCS^{\bullet+}$ provides greater clarity on the fragmentation dynamics, with applications for the analytic mass spectrometry of thiophene and thiophene derivatives. Knowledge about the fragmentation dynamics of thiophene also has implications for the characterization of species relevant to biosynthesis, organic electronics, and the purification of petroleum products. Finally, we have also identified a selective technique for the generation of the thioketene radical cations, $H_2CCS^{\bullet+}$, for use in future reactivity and high-resolution spectroscopy studies. This will allow for the incorporation of $H_2CCS^{\bullet+}$ in models of

25 April 2025 10:13:41

© Author(s) 2025

astrochemical environments such as the cold, dark cloud TMC-1, as well as facilitating future astronomical observations.

SUPPLEMENTARY MATERIAL

The supplementary material contains a detailed comparison of the EI and SIS sources used in this work, further details of the depletion saturation plots, and mass spectra regarding the optimization of tagging parameters, as well as data regarding the laser FWHM. Furthermore, full results for the harmonic and anharmonic frequency calculations are presented, along with a comparison between harmonic and anharmonic calculations as well as different levels of theory, structure of the tagged $H_2CCS^{\bullet+}$ complex, and the geometries of the intermediates and transition states identified in the potential energy surface calculations.

ACKNOWLEDGMENTS

We gratefully acknowledge the support of Radboud University and of NWO for providing beam time at the FELIX Laboratory as well as the skillful assistance of the FELIX staff. We thank the Cologne Laboratory Astrophysics group for providing the FELion ion trap instrument for the current experiments and the Cologne Center for Terahertz Spectroscopy, funded by the Deutsche Forschungsgemeinschaft (DFG, Grant No. SCHL 341/15-1), for supporting its operation.

Furthermore, J.A.D. acknowledges the Department of Physics at the University of Liverpool for Ph.D. scholarship funding. K.S. is supported by the research program "HFML-FELIX: a Dutch Center of Excellence for Science under Extreme Conditions" (with Project No. 184.035.011) of the research program "Nationale Roadmap Grootschalige Wetenschappelijke Infrastructuur," which is financed by the NWO. M.M. acknowledges the Department of Physics at the University of Trento for Ph.D. scholarship funding, as well as COST Action CA21126 - NanoSpace. M.P. acknowledges support from the Ministry of Education, Youth and Sports of the Czech Republic (Grant No. LTC20062). D.A. acknowledges financial support from MUR PRIN 2020 Project No. 2020AFB3FX "Astrochemistry beyond the second period elements" and from the National Recovery and Resilience Plan (NRRP), Mission 4, Component 2, Investment 1.1, Call for Tender No. 1409 published on 14.9.2022 by the Italian Ministry of University and Research (MUR), funded by the European Union–NextGenerationEU–Project Title Grant No. P20223H8CK "Degradation of space-technology polymers by thermospheric oxygen atoms and ions: an exploration of the reaction mechanisms at an atomistic level" - Grant No. CUP E53D23015560001. B.R.H. is grateful to the European Commission (ERC Grant No. 948373), and both B.R.H. and V.R. thank the Leverhulme Trust (Grant No. RPG-2022-264) for funding. The research leading to these results has also received funding from LASERLAB-EUROPE (Grant Agreement No. 871124, European Union's Horizon 2020 research and innovation program).

AUTHOR DECLARATIONS

Conflict of Interest

The authors have no conflicts to disclose.

Author Contributions

J.A.D. and K.S. contributed equally to this work.

Jake A. Diprose: Formal analysis (lead); Investigation (equal); Validation (equal); Visualization (lead); Writing – original draft (equal); Writing – review & editing (equal). **Kim Steenbakkers**: Data curation (equal); Formal analysis (supporting); Investigation (lead); Methodology (supporting); Validation (equal); Visualization (supporting); Writing – original draft (supporting); Writing – review & editing (supporting). **Matteo Michielan**: Investigation (equal); Validation (equal); Writing – review & editing (supporting). **Miroslav Polášek**: Data curation (supporting); Funding acquisition (supporting); Investigation (equal); Resources (equal); Validation (equal); Visualization (supporting); Writing – original draft (supporting); Writing – review & editing (equal). **Daniela Ascenzi**: Conceptualization (equal); Funding acquisition (equal); Investigation (equal); Supervision (supporting); Validation (equal); Writing – original draft (supporting); Writing – review & editing (equal). **Sandra Brünken**: Conceptualization (equal); Funding acquisition (equal); Investigation (equal); Methodology (lead); Project administration (supporting); Resources (lead); Software (equal); Supervision (equal); Validation (equal); Writing – original draft (supporting); Writing – review & editing (equal). **Claire Romanzin**: Conceptualization (equal); Writing – review & editing (supporting). **Brianna R. Heazlewood**: Conceptualization (supporting); Data curation (supporting); Funding acquisition (equal); Resources (supporting); Supervision (supporting); Writing – original draft (supporting); Writing – review & editing (equal). **Vincent Richardson**: Conceptualization (lead); Data curation (equal); Formal analysis (equal); Investigation (equal); Project administration (lead); Supervision (equal); Validation (equal); Visualization (equal); Writing – original draft (equal); Writing – review & editing (lead).

DATA AVAILABILITY

The geometries of the structures used in the PES calculation as well as the predicted line positions and intensities for the various isomers are available either in the manuscript or the supplementary material, with the experimental data used to support the findings of the paper openly available in https://doi.org/10.17638/datacat.liverpool.ac.uk/3011.

REFERENCES

[1]S. R. M. Ibrahim, A. M. Omar, A. A. Bagalagel, R. M. Diri, A. O. Noor, D. M. Almasri, S. G. A. Mohamed, and G. A. Mohamed, "Thiophenes—Naturally occurring plant metabolites: Biological activities and in silico evaluation of their potential as cathepsin D inhibitors," Plants **11**, 539 (2022).

[2]R. Shah and P. K. Verma, "Therapeutic importance of synthetic thiophene," Chem. Cent. J. **12**, 137 (2018).

[3]S. P. Archna, S. Pathania, and P. A. Chawla, "Thiophene-based derivatives as anticancer agents: An overview on decade's work," Bioorg. Chem. **101**, 104026 (2020).

[4]A. Singh, G. Singh, and P. M. S. Bedi, "Thiophene derivatives: A potent multitargeted pharmacological scaffold," J. Heterocycl. Chem. **57**, 2658–2703 (2020).

[5]B. Amna, H. M. Siddiqi, A. Hassan, and T. Ozturk, "Recent developments in the synthesis of regioregular thiophene-based conjugated polymers for electronic and optoelectronic applications using nickel and palladium-based catalytic systems," RSC Adv. **10**, 4322–4396 (2020).

25 April 2025 10:13:41

© Author(s) 2025

[6]J. J. Broughton, S. Patra, M. A. Parkes, G. A. Worth, and H. H. Fielding, "A multiphoton ionisation photoelectron imaging study of thiophene," Phys. Chem. Chem. Phys. **26**, 25461–25468 (2024).
[7]T. A. Saleh, "Characterization, determination and elimination technologies for sulfur from petroleum: Toward cleaner fuel and a safe environment," Trends Environ. Anal. Chem. **25**, e00080 (2020).
[8]A. K. Vasiliou, H. Hu, T. W. Cowell, J. C. Whitman, J. Porterfield, and C. A. Parish, "Modeling oil shale pyrolysis: High-temperature unimolecular decomposition pathways for thiophene," J. Phys. Chem. A **121**, 7655–7666 (2017).
[9]J. Zhao and R. Wang, "Research progress of phase transfer catalysts used in oxidative desulfurization of fuel oil," Mini-Rev. Org. Chem. **18**, 626–648 (2021).
[10]W. Tang, H. Sheng, C. Jin, J. S. Riedeman, and H. I. Kenttämaa, "Characterization of aromatic organosulfur model compounds relevant to fossil fuels by using atmospheric pressure chemical ionization with CS_2 and high-resolution tandem mass spectrometry," Rapid Commun. Mass Spectrom. **30**, 953–962 (2016).
[11]H. P. Upadhyaya, "Theoretical study on the dissociation mechanism of thiophene in the UV photoabsorption, ionization, and electron attachment processes," Int. J. Quantum Chem. **124**, e27503 (2024).
[12]E. Kukk *et al.*, "Formative period in the x-ray-induced photodissociation of organic molecules," Phys. Rev. Res. **3**, 013221 (2021).
[13]P.-K. Lo and K.-C. Lau, "High-level ab initio predictions for the ionization energies and heats of formation of five-membered-ring molecules: Thiophene, furan, pyrrole, 1,3-cyclopentadiene, and borole, $C_4H_4X/C_4H_4X^+$(X = S, O, NH, CH_2, and BH)," J. Phys. Chem. A **115**, 932–939 (2011).
[14]E. E. Rennie, L. Cooper, L. G. Shpinkova, D. M. P. Holland, D. A. Shaw, and P. M. Mayer, "Threshold photoelectron photoion coincidence spectroscopy sheds light on the dissociation of pyrrole and thiophene molecular ions," Int. J. Mass Spectrom. **290**, 142–144 (2010).
[15]E. E. Rennie, D. M. P. Holland, D. A. Shaw, C. A. F. Johnson, and J. E. Parker, "A study of the valence shell spectroscopic and thermodynamic properties of thiophene by photoabsorption and photoion spectroscopy," Chem. Phys. **306**, 295–308 (2004).
[16]H. Lim, D. G. Schultz, E. A. Gislason, and L. Hanley, "Activation energies for the fragmentation of thiophene ions by surface-induced dissociation," J. Phys. Chem. B **102**, 4573–4580 (1998).
[17]R. G. Hayes and W. Eberhardt, "Electron–ion coincidences studies of the fragmentation of thiophene and of tetrahydrothiophene upon core ionization," J. Chem. Phys. **94**, 397–403 (1991).
[18]H. Franke, H. Halim, and H. Schwarz, "Gasphasenchemie metastabiler Thiophen-Radikalkationen," Chem. Ber. **117**, 3194–3204 (1984).
[19]J. J. Butler and T. Baer, "Thermochemistry and dissociation dynamics of state selected C_4H_4X ions. 1. Thiophene," J. Am. Chem. Soc. **102**, 6764–6769 (1980).
[20]M. Lattelais, Y. Ellinger, A. Matrane, and J. C. Guillemin, "Looking for heteroaromatic rings and related isomers as interstellar candidates," Phys. Chem. Chem. Phys. **12**, 4165–4171 (2010).
[21]J. L. Eigenbrode, R. E. Summons, A. Steele, C. Freissinet, M. Millan, R. Navarro-González, B. Sutter, A. C. McAdam, H. B. Franz, D. P. Glavin, P. D. Archer, Jr., P. R. Mahaffy, P. G. Conrad, J. A. Hurowitz, J. P. Grotzinger, S. Gupta, D. W. Ming, D. Y. Sumner, C. Szopa, C. Malespin, A. Buch, and P. Coll, "Organic matter preserved in 3-billion-year-old mudstones at Gale crater, Mars," Science **360**, 1096–1101 (2018).
[22]J. Heinz and D. Schulze-Makuch, "Thiophenes on Mars: Biotic or abiotic origin?," Astrobiology **20**, 552–561 (2020).
[23]R. Simbizi, G. Gahungu, and M. T. Nguyen, "Theoretical investigation of protonated thiophene and two of its nitrile substituted derivatives (2-cyanothiophene and 3-cyanothiophene)," Phys. Chem. Chem. Phys. **22**, 24735–24743 (2020).
[24]M. Agúndez, J. Cernicharo, and M. Guélin, "New molecules in IRC +10216: Confirmation of C_5S and tentative identification of MgCCH, NCCP, and SiH_3CN," Astron. Astrophys. **570**, A45 (2014).
[25]M. B. Bell, L. W. Avery, and P. A. Feldman, "C_3S and C_5S in IRC +10216," The Astrophys. J. **417**, L37 (1993).
[26]J. Cernicharo, C. Cabezas, M. Agúndez, B. Tercero, J. R. Pardo, N. Marcelino, J. D. Gallego, F. Tercero, J. A. López-Pérez, and P. de Vicente, "TMC-1, the starless core sulfur factory: Discovery of NCS, HCCS, H_2CCS, H_2CCCS, and C_4S and detection of C_5S," Astron. Astrophys. **648**, L3 (2021).
[27]J. Cernicharo, M. Guelin, H. Hein, and C. Kahane, "Sulfur in IRC +10216," Astron. Astrophys. **181**, L9–L12 (1987).
[28]B. Tercero, J. Cernicharo, J. R. Pardo, and J. R. Goicoechea, "A line confusion limited millimeter survey of Orion KL I. Sulfur carbon chains," Astron. Astrophys. **517**, A96 (2010).
[29]S. Saito, K. Kawaguchi, S. Yamamoto, M. Ohishi, H. Suzuki, and N. Kaifu, "Laboratory detection and astronomical identification of a new free radical, CCS ($^3\sigma^-$)," Astrophys. J. **317**, L115 (1987).
[30]R. Fuentetaja, M. Agúndez, C. Cabezas, B. Tercero, N. Marcelino, J. R. Pardo, P. de Vicente, and J. Cernicharo, "Discovery of two new interstellar molecules with quijote: HCCCHCCC and HCCCCS," Astron. Astrophys. **667**, L4 (2022).
[31]J. Cernicharo, C. Cabezas, M. Agúndez, R. Fuentetaja, B. Tercero, N. Marcelino, and P. de Vicente, "More sulphur in TMC-1: Discovery of the NC_3S and HC_3S radicals with the quijote line survey," Astron. Astrophys. **688**, L13 (2024).
[32]M. Agúndez, N. Marcelino, J. Cernicharo, and M. Tafalla, "Detection of interstellar HCS and its metastable isomer HSC: New pieces in the puzzle of sulfur chemistry," Astron. Astrophys. **611**, L1 (2018).
[33]M. W. Sinclair, N. Fourikis, J. C. Ribes, B. J. Robinson, R. Brown, and P. D. Godfrey, "Detection of interstellar thioformaldehyde," Aust. J. Phys. **26**, 85 (1973).
[34]J. Cernicharo, C. Cabezas, Y. Endo, N. Marcelino, M. Agúndez, B. Tercero, J. D. Gallego, and P. de Vicente, "Space and laboratory discovery of HC_3S^+," Astron. Astrophys. **646**, L3 (2021).
[35]C. Cabezas, M. Agúndez, N. Marcelino, B. Tercero, Y. Endo, R. Fuentetaja, J. R. Pardo, P. de Vicente, and J. Cernicharo, "Discovery of the elusive thioketenylium, $HCCS^+$, in TMC-1," Astron. Astrophys. **657**, L4 (2022).
[36]B. A. McGuire, C. N. Shingledecker, E. R. Willis, K. L. Kelvin Lee, M.-A. Martin-Drumel, G. A. Blake, C. L. Brogan, A. M. Burkhardt, P. Caselli, K.-J. Chuang, S. El-Abd, T. R. Hunter, S. Ioppolo, H. Linnartz, A. J. Remijan, C. Xue, and M. C. McCarthy, "Searches for interstellar HCCSH and H_2CCS," Astrophys. J. **883**, 201 (2019).
[37]P. Rosmus, B. Solouki, and H. Bock, "Ground and excited states of thioketene radical cation, H_2CCS^+," Chem. Phys. **22**, 453–458 (1977).
[38]H. Bock, B. Solouki, G. Bert, and P. Rosmus, "Unstable intermediates. 5. Thioketene," J. Am. Chem. Soc. **99**, 1663–1664 (1977).
[39]J. Kreile, H.-D. Kurland, W. Seibel, and A. Schweig, "Photoelectron angular distribution parameters of valence shell ionizations of allene and transient ketene and thioketene," J. Mol. Struct. **300**, 149–156 (1993).
[40]T. M. Orlando, B. Yang, Y.-h. Chiu, and S. L. Anderson, "The effects of different vibrational modes and collision energy on the reaction of acetylene cations with carbonyl sulfide," J. Chem. Phys. **92**, 7356–7364 (1990).
[41]T. M. Orlando, A. Friedmann, and J. P. Maier, "Photodissociation spectroscopy of the $[OCS \bullet C_2H_2]^+$ cluster ion," J. Chem. Phys. **92**, 7365–7372 (1990).
[42]B. Yang, Y.-h. Chiu, and S. L. Anderson, "The effects of reactant vibrational, fine structure, and collision energy on the reactions of OCS^+ with C_2H_2: Complementary studies of reactions in the $[C_2H_2+OCS]^+$ system," J. Chem. Phys. **94**, 6459–6468 (1991).
[43]Y.-h. Chiu, H. Fu, J.-t. Huang, and S. L. Anderson, "Reaction mechanisms and energy disposal in the $[C_2H_2{:}OCS]^+$ system: A mode-selective differential cross section study," J. Chem. Phys. **105**, 3089–3107 (1996).
[44]F. Muntean and P. B. Armentrout, "Collision-induced dissociation dynamics of the $[OCS \bullet C_2H_2]^+$ complex: A combined experimental and theoretical study," Z. Phys. Chem. **214**, 103521063 (2000).
[45]H. Li, J. Lang, C. D. Foley, J. Zádor, and A. G. Suits, "Sulfur (^{3}P) reaction with conjugated dienes gives cyclization to thiophenes under single collision conditions," J. Phys. Chem. Lett. **14**, 7611–7617 (2023).
[46]J. Lang, C. D. Foley, S. Thawoos, A. Behzadfar, Y. Liu, J. Zádor, and A. G. Suits, "Reaction dynamics of S(^{3}P) with 1,3-butadiene and isoprene: Crossed-beam scattering, low-temperature flow experiments, and high-level electronic structure calculations," Faraday Discuss. **251**, 550–572 (2024).
[47]J. Holmes, C. Aubry, and P. Mayer, *Assigning Structures to Ions in Mass Spectrometry* (CRC Press, Taylor and Francis Group, Boca Raton, FL, 2006).
[48]S. T. Graul and M. T. Bowers, "Dynamics of metastable dissociation and photodissociation of the gas-phase cluster ion $(OCS{:}C_2H_2)^+$," J. Phys. Chem. **95**, 8328–8337 (1991).

25 April 2025 10:13:41

© Author(s) 2025

[49]S. Thorwirth, M. E. Harding, O. Asvany, S. Brünken, P. Jusko, K. L. K. Lee, T. Salomon, M. C. McCarthy, and S. Schlemmer, "Descendant of the X-ogen carrier and a 'mass of 69': Infrared action spectroscopic detection of HC_3O^+ and HC_3S^+," Mol. Phys. **118**, e1776409 (2020).
[50]D. Oepts, A. F. G. van der Meer, and P. W. van Amersfoort, "The free-electron-laser user facility FELIX," Infrared Phys. Technol. **36**, 297–308 (1995).
[51]P. Jusko, S. Brünken, O. Asvany, S. Thorwirth, A. Stoffels, L. van der Meer, G. Berden, B. Redlich, J. Oomens, and S. Schlemmer, "The FELion cryogenic ion trap beam line at the FELIX free-electron laser laboratory: Infrared signatures of primary alcohol cations," Faraday Discuss. **217**, 172–202 (2019).
[52]D. Gerlich, "Inhomogeneous RF fields: A versatile tool for the study of processes with slow ions," in *State-Selected and State-to-State Ion-Molecule Reaction Dynamics. Part 1: Experiment*, Advances in Chemical Physics Series Vol. LXXXII, edited by C.-Y. Ng and M. Baer (John Wiley & Sons, Inc., 1992), ISBN: 0-471-53258-4 CD.
[53]O. Asvany, F. Bielau, D. Moratschke, J. Krause, and S. Schlemmer, "Note: New design of a cryogenic linear radio frequency multipole trap," Rev. Sci. Instrum. **81**, 076102 (2010).
[54]A. N. Marimuthu, D. Sundelin, S. Thorwirth, B. Redlich, W. D. Geppert, and S. Brünken, "Laboratory gas-phase vibrational spectra of $[C_3H_3]^+$ isomers and isotopologues by IRPD spectroscopy isomers and isotopologues by irpd spectroscopy," J. Mol. Spectrosc. **374**, 111377 (2020).
[55]M. J. Frisch *et al.,* Gaussian 16, Revision C.01, Gaussian, Inc., Wallingford, CT, 2016.
[56]P. J. Linstrom and W. G. Mallard, "NIST chemistry WebBook—Standard reference database No. 69," [Online] (accessed April 2024).
[57]J. Yang, J. Li, and Y. Mo, "The vibrational structures of furan, pyrrole, and thiophene cations studied by zero kinetic energy photoelectron spectroscopy," J. Chem. Phys. **125**, 174313 (2006).
[58]Y.-S. Cheung, J.-C. Huang, and C. Y. Ng, "Vacuum ultraviolet laser pulsed field ionization photoelectron studies of polyatomic species: Accurate ionization energies of CH_3SH and CH_3CH_2SH," J. Chem. Phys. **109**, 1781–1786 (1998).
[59]S. Choi, K.-W. Choi, S. K. Kim, S. Chung, and S. Lee, "Vibrational structures of dimethyl sulfide and ethylene sulfide cations studied by vacuum-ultraviolet mass-analyzed threshold ionization (MATI) spectroscopy," J. Phys. Chem. A **110**, 13183–13187 (2006).
[60]T. H. Dunning, Jr., "Gaussian basis sets for use in correlated molecular calculations. I. The atoms boron through neon and hydrogen," J. Chem. Phys. **90**, 1007–1023 (1989).
[61]D. E. Woon and T. H. Dunning, Jr., "Gaussian basis sets for use in correlated molecular calculations. III. The atoms aluminum through argon," J. Chem. Phys. **98**, 1358–1371 (1993).
[62]NIST, "III.B.3.a. (XIII.C.1.) precomputed vibrational scaling factors," (2013); accessed 4 April 2024.
[63]H.-J. Werner, P. J. Knowles, G. Knizia, F. R. Manby, and M. Schütz, "Molpro: A general-purpose quantum chemistry program package," WIREs Comput. Mol. Sci. **2**, 242–253 (2012).
[64]H.-J. Werner, P. J. Knowles, F. R. Manby, J. A. Black, K. Doll, A. Heßelmann, D. Kats, A. Köhn, T. Korona, D. A. Kreplin *et al.*, "The Molpro quantum chemistry package," J. Chem. Phys. **152**, 144107 (2020).
[65]R. A. Kendall, T. H. Dunning, and R. J. Harrison, "Electron affinities of the first-row atoms revisited. Systematic basis sets and wave functions," J. Chem. Phys. **96**, 6796–6806 (1992).
[66]Z. Szilágyi and K. Vékey, "A simple algorithm for the calculation of kinetic energy release distributions," Eur. Mass Spectrom. **1**, 507–518 (1995).

25 April 2025 10:13:41

© Author(s) 2025